JoT JOURNAL OF TURBULENCE

http://jot.iop.org/

On modal time correlations of turbulent velocity and scalar fields

P A O'Gorman and D I Pullin

Graduate Aeronautical Laboratories 105-50, California Institute of Technology, Pasadena, CA 91125, USA
E-mail: pog@caltech.edu

Received 26 February 2004
Published 17 September 2004
doi:10.1088/1468-5248/5/1/035

Abstract. We consider Eulerian two-point, two-time correlations of a turbulent velocity field and those of a passive scalar mixed by a turbulent velocity field. Integral expressions are derived for the modal time-correlation functions of the velocity and scalar fields using the stretched-spiral vortex model. These expressions are evaluated using asymptotic methods for high wavenumber and, alternatively, using numerical integration. If the motion of the centres of the vortex structures is neglected, then an inertial time scaling $(\epsilon k^2)^{-1/3}$, where ϵ is the energy dissipation rate and k the wavenumber, is found to collapse the velocity and scalar modal time-correlation functions to universal forms. Allowing the centres of the vortex structures to move introduces a sweeping time scale, $(uk)^{-1}$, where u is the rms velocity of the centres of the vortex structures. The sweeping time scale dominates the inertial time scale for sufficiently large wavenumbers. Results are also reported for a direct numerical simulation of passive scalar mixing by a turbulent velocity field at a Taylor Reynolds number of 265. The velocity and scalar modal time-correlation functions were calculated in the simulation. They coincide for large enough wavenumbers and are found to collapse to universal forms when a sweeping time scale is used.

PACS numbers: 47.27.Eq, 47.32.Cc

JoT 5 (2004) 035

 PII: S1468-5248(04)76871-5 1468-5248/04/000001+21$30.00

Contents

1. Introduction

A fundamental but still disputed property of isotropic, homogeneous turbulence is the characteristic time scale over which the small scales of the velocity field decorrelate in an Eulerian frame of reference. Kolmogorov scaling in the inertial range suggests the inertial eddy-turnover time, $(\epsilon k^2)^{-1/3}$, where ϵ is the energy dissipation rate and k the wavenumber. There is, however, also evidence that the relevant time scale is the 'sweeping' time, $(u_{rms}k)^{-1}$, where u_{rms} is the rms velocity [1]–[5]. Knowledge of the correct time scaling would be useful, for example, as an input to the recent functional derivative closure (FDC) [6] for random advection of a passive scalar, and for interpreting the importance of the random sweeping effect [1]. In addition, Eulerian decorrelation time scales are important in the problem of sound generation by turbulence (see [7]). Also of interest is the characteristic time scale of the small scales of a passive scalar mixed by a turbulent velocity field.

The velocity modal time correlations are the time correlations of the Fourier modes of the velocity field and so are a two-time, two-point statistic. Several attempts have been made to use characteristic time scalings to collapse these correlations to a universal form. The main experimental work is by Comte-Bellot and Corrsin [8] in decaying grid turbulence and is at a maximum Taylor Reynolds number R_λ of 72. They achieved a collapse of the modal time correlations using a parallel combination of four different characteristic time scales. DNS studies by Orszag and Patterson [2] at $R_\lambda \sim 16$, by Gotoh *et al* [3] at $R_\lambda \sim 46$, by Kaneda *et al* [4] at $R_\lambda \sim 126$ and by Sanada and Shanmugasundaram [1] at $R_\lambda \sim 200$, all found the 'sweeping' time scale to be dominant.

Kraichnan [5], studied the modal time correlations and made a simple linearized estimate and also an estimate based on the direct interaction approximation (DIA), both of which resulted in the 'sweeping' time being the characteristic time scale. McComb *et al* [9] studied numerical solutions to the DIA and local energy transfer (LET) theories and, in contrast to Kraichnan's asymptotic prediction for the DIA, found that while neither the 'sweeping' time scale nor the inertial eddy-turnover time scale were completely effective in collapsing the modal time-correlation data, the inertial scaling became more dominant for both theories as R_λ was increased. Finally, Gotoh *et al* [3] studied the modal time correlation using both DNS and DIA at $R_\lambda \sim 35$ and found that the sweeping time scale gave a poor collapse of the correlation data from the DIA relative to the data from the DNS.

The sweeping effect is also found to be important for the Eulerian frequency spectrum of turbulence. Tennekes [10] studied this one-point, two-time statistic and found a simple relation between the Eulerian frequency spectrum and the energy spectrum using a sweeping hypothesis. Malik and Vassilicos [11] found this relation to be valid for a number of different types of randomly advected vortex tubes, including a particular realization of an inviscid Lundgren spiral vortex sheet. Finally, Yeung and Sawford [12] extended the study of the Eulerian frequency spectrum and random sweeping to the passive scalar and found that the Tennekes relation between frequency and wavenumber spectra gave similarly shaped spectra for the scalar. Here, we will study the modal time-correlation function, which differs from the Eulerian frequency spectrum in that it gives the time correlation at a particular length scale.

The stretched-spiral vortex model of turbulence, introduced by Lundgren [13], uses an ensemble of tube-like vortex structures to model the fine scales of turbulence. The vortex tubes are assumed to be straight, with no dependence of the velocity field on the coordinate parallel to the tube axis. The vortex tubes do not interact with each other, except that they are stretched on average by the surrounding flow. In each structure, the vorticity is evolved by the Navier–Stokes equations using a solution that is asymptotically correct for large time. The non-axisymmetric part of the vorticity is wound up into a spiral by the differential rotation of the cores of the vortices. The vortex structures are continuously created by a process external to the model, such as vortex coalescence. Each structure then decays over time, so that a statistically stationary state is reached. Average flow statistics are initially interpreted as an average over all space, including, at any instant, many different structures at different times in their evolution. An ergodic hypothesis is then invoked to convert this volume average over all space to a volume and time average of an ensemble of individual structures with different orientations. In the case of the vorticity field, where much of the intense vorticity is concentrated in localized regions [14], neglect of the overlapping regions of the vortex structures is reasonable; however, for the scalar and axial velocity fields, this approximation is more difficult to justify.

The stretched-spiral vortex model gives results in agreement with classical scaling arguments for one-time, two-point statistics, such as the energy spectrum [13] and the scalar spectrum [15]. By also performing an average over vortex orientation, the model was used to calculate vorticity and velocity-derivative moments [16], one-dimensional spectra [17] and the velocity-scalar cross spectrum [18]. The model has also been extended to the compressible case (see [19]).

Here, we will use this model to calculate the modal time correlations of the velocity field, as well as the modal time correlations of a passive scalar field. We also report the results of a high-resolution (512^3) direct numerical simulation of turbulent mixing of a passive scalar by forced box turbulence, including results for the modal time correlations of the velocity and the scalar. The DNS results are compared with the theoretical results of the stretched-spiral vortex model.

In section 2, we define the modal time-correlation functions for the velocity and the scalar and briefly discuss some of their properties. Expressions for these functions are derived using

the stretched-spiral vortex model in sections 3.1 and 3.2, and these expressions are evaluated asymptotically in section 3.3 and numerically in section 3.4. The effect of motion of the centres of the vortex structures is considered in section 3.5. Finally, in section 4, the DNS results are reported and compared with the stretched-spiral vortex model.

2. The modal time-correlation function

We consider homogeneous turbulence and begin by defining the two-time, two-point velocity correlation at time t by

$$\mathcal{R}_{ij}(\mathbf{r},t,\sigma) = \overline{u_i(\mathbf{x},t)u_j(\mathbf{x}+\mathbf{r},t+\sigma)}, \tag{1}$$

where the overbar is taken to be an ensemble average. Then, the shell-summed two-time velocity cross-spectrum at time t is defined by

$$Q_{ij}(k,t,\sigma) = \frac{1}{(2\pi)^3}\int_S\int_V \mathcal{R}_{ij}(\mathbf{r},t,\sigma)\mathrm{e}^{-\mathrm{i}\mathbf{k}\cdot\mathbf{r}}\,\mathrm{d}\mathbf{r}\,\mathrm{d}\Omega_k, \tag{2}$$

where the integral over V indicates a volume integral over all space and the integral over S indicates a surface integral over a spherical shell in wavenumber space. Note that this shell average in wavenumber ensures that $Q_{ij}(k,t,\sigma)$ is a real quantity. The usual shell-summed energy spectrum is given by $E(k,t) = 1/2\,Q_{jj}(k,t,0)$, where the summation over j is implied. The modal time-correlation function at time t, $R(k,t,\sigma)$, is then defined by (see [8])

$$R(k,t,\sigma) = \frac{Q_{jj}(k,t,\sigma)}{2\left(E(k,t)E(k,t+\sigma)\right)^{1/2}}, \tag{3}$$

so that $R(k,t,0) = 1$. It is straightforward to show that

$$\frac{\partial}{\partial\sigma}R(k,t,\sigma)\bigg|_{\sigma=0} = 0, \tag{4}$$

even when the turbulence is non-stationary (see appendx A). We will be concerned with the case of stationary turbulence, so that we may omit references to t and define

$$R(k,\sigma) = \frac{Q_{jj}(k,\sigma)}{2E(k)}. \tag{5}$$

Similarly, for a passive scalar $c(\mathbf{x},t)$, we define the two-point, two-time scalar correlation function $\mathcal{R}^c(\mathbf{r},\sigma)$ by

$$\mathcal{R}^c(\mathbf{r},\sigma) = \overline{c(\mathbf{x},t)c(\mathbf{x}+\mathbf{r},t+\sigma)}, \tag{6}$$

the shell-summed, two-time scalar cross-spectrum $Q^c(k,\sigma)$ by

$$Q^c(k,\sigma) = \frac{1}{(2\pi)^3}\int_S\int_V \mathcal{R}^c(\mathbf{r},\sigma)\mathrm{e}^{-\mathrm{i}\mathbf{k}\cdot\mathbf{r}}\,\mathrm{d}\mathbf{r}\,\mathrm{d}\Omega_k, \tag{7}$$

and the scalar modal time-correlation function $R^c(k,\sigma)$ by

$$R^c(k,\sigma) = \frac{Q^c(k,\sigma)}{E^c(k)}, \tag{8}$$

where $E^c(k) = Q^c(k,0)$ is the scalar power spectrum. It is easily verified that the property $(\partial/\partial\sigma)R^c(k,\sigma)|_{\sigma=0} = 0$ also holds.

3. Application of the stretched-spiral vortex model

We wish to calculate the modal correlation functions using the stretched-spiral vortex model. For the moment, we will assume that the centres of the vortex structures are stationary; the velocity and scalar modal correlation functions will be denoted $\tilde{R}(k,\sigma)$ and $\tilde{R}^c(k,\sigma)$ respectively in this case. Gross motion of the vortex structures will be considered in section 3.5.

3.1. Modal time correlations of stretched vortex structures

Here, we will calculate $\tilde{R}(k,\sigma)$ and $\tilde{R}^c(k,\sigma)$ for a collection of stretched vortex structures. To perform the simplest possible analysis, at least as a first step, we assume that the velocity and scalar fields in each vortex structure have no dependence on the axial coordinate. For the same reason, we neglect the contribution from the axial velocity, and we consider the statistically isotropic case, without a mean scalar gradient. See O'Gorman and Pullin [18] for an example of the inclusion of effects of a mean scalar gradient in the stretched-spiral vortex model.

Each vortex structure is embedded in an axisymmetric background strain field, characterized by a strain rate a. The strain field is assumed to arise as a result of the other vortex structures, and it is important because it allows the model to include the phenomenon of vorticity enhancement by stretching. The velocity field in a typical stretched vortex tube may then be decomposed as

$$u_i = v_i(x_1, x_2, t) + a_i(t)x_i, \tag{9}$$

where summation over i is not implied, $a_1 = a_2 = -a/2$, $a_3 = a$, $a > 0$, and the strain rate a is assumed constant. Note that we are now working with coordinates centred in the vortex structure and with the x_3 direction aligned with the vortex axis. We will make use of the two-dimensional Fourier transform of the velocity field, $\hat{v}_j(k_1, k_2, t)$, defined by

$$\hat{v}_j(k_1,k_2,t) = \frac{1}{4\pi^2}\int_{-\infty}^{\infty}\int_{-\infty}^{\infty} \mathrm{e}^{-\mathrm{i}k_1x_1-\mathrm{i}k_2x_2} v_j(x_1,x_2,t)\,\mathrm{d}x_1\,\mathrm{d}x_2, \tag{10}$$

and similarly for the scalar field.

As discussed in section 1, we now interpret the ensemble average in the definition of the modal time-correlation functions as a volume average over all space, which we then convert, by means of an ergodic hypothesis, to a volume, time and orientation average for a single vortex structure. Further details and discussion of the interpretation of this averaging process may be found in [13]. Our starting point is equation (B16) from Pullin and Saffman [16] for a general cross-spectrum, applied to $Q_{jj}(k,\sigma)$ and $Q^c(k,\sigma)$ and modified to include a time average over the lifetime of the vortex,

$$Q_{jj}(k,\sigma) = 4\pi^2 Nk \int_0^{\infty}\int_0^{2\pi} \hat{v}_j(k_1,k_2,t)\hat{v}_j^*(k_1,k_2,t+\sigma)\,\mathrm{d}\theta_k\,S(t)\,\mathrm{d}t, \tag{11}$$

$$Q^c(k,\sigma) = 4\pi^2 Nk \int_0^{\infty}\int_0^{2\pi} \hat{c}(k_1,k_2,t)\hat{c}^*(k_1,k_2,t+\sigma)\,\mathrm{d}\theta_k\,S(t)\,\mathrm{d}t, \tag{12}$$

where $k_1 = k\cos\theta_k$ and $k_2 = k\sin\theta_k$. Here, $S(t) = \exp(at)$ is a stretching factor due to the uniform strain rate a and N is the rate of creation of vortex tube length per unit time and per unit volume. Note that the stretching factor is $S(t)$ rather than $S(t+\sigma)$, since we take the length of the shorter tube when considering correlations between two tubes of different lengths.

We must now decide on an appropriate expression for $E(k)$ in the definition of $\tilde{R}(k,\sigma)$ (equation (5)). Guided by the definition of $\tilde{R}(k,t,\sigma)$ for non-stationary turbulence, we take a

geometric average of the energy spectra associated with the velocity fields starting from $t = 0$ and σ,

$$E(k) = \left(2\pi^2 Nk \int_0^\infty \int_0^{2\pi} \hat{v}_j(k_1, k_2, t)\hat{v}_j^*(k_1, k_2, t)\,\mathrm{d}\theta_k\, S(t)\,\mathrm{d}t\right)^{1/2} \times \left(2\pi^2 Nk \int_0^\infty \int_0^{2\pi} \hat{v}_j(k_1, k_2, t+\sigma)\hat{v}_j^*(k_1, k_2, t+\sigma)\,\mathrm{d}\theta_k\, S(t)\,\mathrm{d}t\right)^{1/2}. \tag{13}$$

Note that we choose $S(t)$ rather than $S(t+\sigma)$ in the second term in parentheses, so that N is still the correct normalization factor. It is straightforward to check that when expressions (11) and (13) are used in definition (5), then property (4) remains valid. Similarly, we choose

$$E^c(k) = \left(4\pi^2 Nk \int_0^\infty \int_0^{2\pi} \hat{c}(k_1, k_2, t)\hat{c}^*(k_1, k_2, t)\,\mathrm{d}\theta_k\, S(t)\,\mathrm{d}t\right)^{1/2} \times \left(4\pi^2 Nk \int_0^\infty \int_0^{2\pi} \hat{c}(k_1, k_2, t+\sigma)\hat{c}^*(k_1, k_2, t+\sigma)\,\mathrm{d}\theta_k\, S(t)\,\mathrm{d}t\right)^{1/2}. \tag{14}$$

If the velocity field of the vortex decays sufficiently fast away from the origin, we have that $\hat{v}_l(k_1, k_2, t) = \mathrm{i}\,k^{-2}\epsilon_{lmn}k_m\hat{\omega}_n(k_1, k_2, t)$, where $\omega_i(x_1, x_2, t)$ is the vorticity field and $\hat{\omega}_i(k_1, k_2, t)$ its Fourier transform. Assuming that $\omega_1 = \omega_2 = 0$ and using $k_l\hat{\omega}_l = 0$, it is then easy to show from equations (5) and (11) that

$$\tilde{R}(k, \sigma)E(k) = \frac{1}{k}2\pi^2 N \int_0^\infty \int_0^{2\pi} \hat{\omega}_3(k_1, k_2, t)\hat{\omega}_3^*(k_1, k_2, t+\sigma)\,\mathrm{d}\theta_k\, S(t)\,\mathrm{d}t, \tag{15}$$

where $E(k)$ is given by

$$E(k) = \left(\frac{1}{k}2\pi^2 N \int_0^\infty \int_0^{2\pi} \hat{\omega}_3(k_1, k_2, t)\hat{\omega}_3^*(k_1, k_2, t)\,\mathrm{d}\theta_k\, S(t)\,\mathrm{d}t\right)^{1/2} \times \left(\frac{1}{k}2\pi^2 N \int_0^\infty \int_0^{2\pi} \hat{\omega}_3(k_1, k_2, t+\sigma)\hat{\omega}_3^*(k_1, k_2, t+\sigma)\,\mathrm{d}\theta_k\, S(t)\,\mathrm{d}t\right)^{1/2}. \tag{16}$$

We now decompose $\omega_3(r, \theta, t)$ as $\omega_3(r, \theta, t) = \sum_{n=-\infty}^{\infty} \omega_n(r, t)\exp(\mathrm{i}n\theta)$, where $\omega_n(r, t) = \omega_{-n}^*(r, t)$. The identity

$$\int_0^{2\pi} \exp(\mathrm{i}n\theta - \mathrm{i}kr\cos(\theta - \theta_k))\,\mathrm{d}\theta = (-\mathrm{i})^n 2\pi J_n(kr)\exp(\mathrm{i}n\theta_k), \tag{17}$$

can then be used to give

$$\hat{\omega}_3(k, \theta_k, t) = \frac{1}{2\pi}\sum_{n=-\infty}^{\infty} (-\mathrm{i})^n \exp(\mathrm{i}n\theta_k)I_n(k, t), \tag{18}$$

where

$$I_n(k, t) = \int_0^\infty \omega_n(r, t)J_n(kr)r\,\mathrm{d}r. \tag{19}$$

Then, we have that

$$\tilde{R}(k, \sigma) = \frac{\sum_{n=-\infty}^{\infty} \int_0^\infty I_n(k, t)I_n^*(k, t+\sigma)S(t)\,\mathrm{d}t}{(\sum_{n=-\infty}^{\infty} A_n(k, \sigma))^{1/2}(\sum_{n=-\infty}^{\infty} A_n(k, 0))^{1/2}}, \tag{20}$$

where

$$A_n(k,\sigma) = \int_0^\infty |I_n(k,t+\sigma)|^2 S(t)\,\mathrm{d}t. \tag{21}$$

This can be simplified by using $I_{-n} = I_n^*(-1)^n$ to give that $I_{-n}(k,t)I_{-n}^*(k,t+\sigma) = I_n^*(k,t)I_n(k,t+\sigma)$. Omitting the zeroth harmonic contribution, we have that

$$\tilde{R}(k,\sigma) = \frac{\sum_{n=1}^\infty \int_0^\infty Re(I_n(k,t)I_n^*(k,t+\sigma))S(t)\,\mathrm{d}t}{(\sum_{n=1}^\infty A_n(k,\sigma))^{1/2}(\sum_{n=1}^\infty A_n(k,0))^{1/2}}. \tag{22}$$

Similarly for the passive scalar,

$$\tilde{R}^c(k,\sigma) = \frac{\sum_{n=1}^\infty \int_0^\infty Re(I_n^c(k,t)I_n^{c*}(k,t+\sigma))S(t)\,\mathrm{d}t}{(\sum_{n=1}^\infty A_n^c(k,\sigma))^{1/2}(\sum_{n=1}^\infty A_n^c(k,0))^{1/2}}, \tag{23}$$

where $c(r,\theta,t) = \sum_{n=-\infty}^\infty c_n(r,t)\exp(\mathrm{i}\,n\theta)$, and A_n^c and I_n^c are defined by replacing ω_n with c_n in equation (19) and I_n with I_n^c in equation (21).

3.2. Use of the stretched spiral solutions

To evaluate expressions (22) and (23) for $\tilde{R}(k,\sigma)$ and $\tilde{R}^c(k,\sigma)$ respectively, we need to specify solutions for $\omega_n(r,t)$ and $c_n(r,t)$. The stretched-spiral vortex model uses solutions of the Navier–Stokes equations and the advection–diffusion equation that are asymptotically accurate for large time. These solutions capture the winding up over time of the non-axisymmetric component of the vorticity and scalar fields.

Following Lundgren [13], we introduce the stretched coordinates, ρ and τ, given by

$$\rho = S(t)^{1/2}r, \qquad \tau = \frac{1}{a}(S(t)-1). \tag{24}$$

Lundgren has shown that, given any solution $\omega^{2d}(\rho,\theta,\tau)$ to the (unstretched) two-dimensional vorticity equation, a corresponding solution for the vorticity in the stretched vortex tube is given by $\omega_3(r,\theta,t) = S(t)\omega^{2d}(\rho,\theta,\tau)$. It was also shown that the non-axisymmetric part of $\omega^{2d}(\rho,\theta,\tau)$ evolves on much faster time scales compared with the axisymmetric component, so that we can make the approximation that the zeroth harmonic, $\omega_0^{2d}(\rho)$, is independent of τ. The azimuthally averaged angular velocity $\Omega(\rho)$ is related to $\omega_0^{2d}(\rho)$ by

$$\omega_0^{2d} = \frac{1}{\rho}\frac{\partial(r^2\Omega)}{\partial\rho}, \tag{25}$$

and we also define the derivative $\Lambda(\rho) = \mathrm{d}\Omega(\rho)/\mathrm{d}\rho$. Then, the following approximate solution to the Navier–Stokes equations is asymptotically accurate for large time:

$$\omega_n(r,t) = S(t)f_n(\rho)\exp(-\mathrm{i}n\Omega(\rho)\tau - \nu n^2\Lambda(\rho)^2\tau^3/3), \quad n \geq 1. \tag{26}$$

Here, ν is the viscosity, and the arbitrary functions $f_n(\rho)$ specify the initial condition of the vorticity.

The scalar differs from the vorticity in that it is not amplified by stretching, and it can be shown that [15]

$$c_n(r,t) = g_n(\rho)\exp(-\mathrm{i}n\Omega(\rho)\tau - Dn^2\Lambda(\rho)^2\tau^3/3), \quad n \geq 1 \tag{27}$$

is a solution to the scalar advection–diffusion equation, asymptotically accurate for large time, where D is the diffusivity and $g_n(\rho)$ are arbitrary functions specifying the initial condition for the scalar.

To find quantitative results for $\tilde{R}(k,\sigma)$ and $\tilde{R}^c(k,\sigma)$, it will be necessary to specify the functions $f_n(\rho)$, $g_n(\rho)$ and $\Omega(\rho)$, as well as the strain rate a. The viscosity and diffusivity may be regarded as external parameters. One strength of the stretched-spiral vortex model is that many flow statistics show a universal character, independent of specific choices for $f_n(\rho)$, $g_n(\rho)$, $\Omega(\rho)$ and a. For example, Lundgren [13] showed that the form of the wavenumber dependence of the energy spectrum resulting from the stretched-spiral vortex model was independent of the specific choice of these quantities. At the same time, since there are many internal parameters in the model, the resulting expressions are not solely determined by dimensional analysis.

3.3. Asymptotic evaluation

We will now use an asymptotic analysis to evaluate the expressions (22) and (23) for $\tilde{R}(k,\sigma)$ and $\tilde{R}^c(k,\sigma)$, respectively. Firstly, we concentrate on $\tilde{R}(k,\sigma)$ and use the method of stationary phase to evaluate $I_n(k,t)$ for large wavenumber and large time [13]:

$$\begin{aligned} I_n(k,t) &= \int_0^\infty J_n\left(\frac{k\rho}{(1+a\tau)^{1/2}}\right) f_n(\rho)\exp(-\mathrm{i}n\Omega(\rho)\tau - \nu n^2\Lambda(\rho)^2\tau^3/3)\rho\,\mathrm{d}\rho \\ &\simeq (1+a\tau)^{1/4}k^{-1/2}\rho_s^{1/2}f_n(\rho_s)(n\Delta(\rho_s)\tau)^{-1/2}\mathrm{i}^{n+1/2} \\ &\quad\times\exp(\mathrm{i}(-k\rho_s(1+a\tau)^{-1/2} - n\Omega(\rho_s)\tau - \pi/4) - n^2\tau^3\nu\Lambda^2(\rho_s)/3), \end{aligned} \tag{28}$$

where we have assumed $\Lambda(\rho)$ is monotonic, $\Delta(\rho) = \mathrm{d}\Lambda(\rho)/\mathrm{d}\rho$ and the point of stationary phase ρ_s is given by $k + n\Lambda(\rho_s)\tau(1+a\tau)^{1/2} = 0$. Furthermore, assuming that only large $(a\tau)$ will be important gives

$$kn^{-1}\Lambda(\rho_s)^{-1}a^{-1/2}\tau^{-3/2} = 1 + \mathrm{O}\left(\frac{1}{a\tau}\right). \tag{29}$$

The integral $I_n(k,t+\sigma)$ is approximated by the right-hand side of equation (28) evaluated at $t+\sigma$, so that τ is replaced by

$$\tau' = \frac{1}{a}(\mathrm{e}^{a\sigma}(a\tau+1) - 1), \tag{30}$$

and ρ_s is replaced by ρ_s', where $k + n\Lambda(\rho_s')\tau'(1+a\tau')^{1/2} = 0$. Noting that $\Lambda^2(\rho_s')\tau'^3 \simeq \Lambda^2(\rho_s)\tau^3$ for a given n and k implies that the viscous parts of $I_n(k,t)$ and $I_n(k,t+\sigma)$ are similar for large $(a\tau)$.

We now restrict the range of delay times σ that we are concerned with, so that we can relate $I_n(k,t+\sigma)$ to $I_n(k,\sigma)$. Let L be the characteristic length scale for $\Omega(\rho)$, and for simplicity, assume, that this is the same for $f_n(\rho)$. We then restrict attention to the range $(k\,L)^{2/3}(a\sigma)^2 \ll 1$ and $(k\,L) \gg 1$, so that $(a\sigma) \ll 1$. This corresponds to length scales smaller than the characteristic size of the vortex structure and to time scales smaller than the stretching time of the background strain field. However, $(kL)^{2/3}(a\sigma)$ is assumed to be of order one or greater. Then, to leading order $\rho_s' \simeq \rho_s$, $f_n(\rho_s') \simeq f_n(\rho_s)$, $\tau_s' \simeq \tau_s$ and $\Delta(\rho_s') \simeq \Delta(\rho_s)$, where higher-order terms are a factor $(a\sigma)$ smaller in magnitude. However, care must be taken with the argument of the complex exponential in equation (28), $h_n(\rho) = -k\rho_s(a\tau)^{-1/2} - n\Omega(\rho_s)\tau$. When we substitute our asymptotic expressions for $I_n(k,t)$ and $I_n(k,t+\sigma)$ in the numerator

of equation (22) for $\tilde{R}(k,\sigma)$, then $(h_n(\rho_s') - h_n(\rho_s))$ cannot be neglected. By changing the integration variables from t to ρ_s in equation (22), we find that

$$\tilde{R}(k,\sigma) \simeq \frac{\sum_{n=1}^{\infty} n^{-4/3} \int_0^{\infty} \Lambda(\rho_s)^{-4/3} |f_n(\rho_s)|^2 \rho_s \cos(h_n(\rho_s') - h_n(\rho_s))\, \mathrm{d}\rho_s}{\sum_{n=1}^{\infty} n^{-4/3} \int_0^{\infty} \Lambda(\rho_s)^{-4/3} |f_n(\rho_s)|^2 \rho_s \, \mathrm{d}\rho_s}. \tag{31}$$

The viscous parts of $I_n(k, t+\sigma)$ and $I_n(k,t)$ are identical and independent of t to within the current approximation and so factor out.

It remains to find $h_n(\rho_s') - h_n(\rho_s)$ to leading order (see appendix B). The result is

$$h_n(\rho_s') - h_n(\rho_s) = k^{2/3} \sigma n^{1/3} a^{2/3} s(\rho_s) + \mathrm{O}((kL)^{2/3}(a\sigma)^2) + \mathrm{O}(a\sigma), \tag{32}$$

where

$$s(\rho_s) = \left(\frac{|\Lambda(\rho_s)|^{1/3} \rho_s}{2} - \frac{\Omega(\rho)}{|\Lambda(\rho_s)|^{2/3}} \right). \tag{33}$$

The analysis in appendix B shows that the first term in (33) is related to the radial motion due to stretching in time σ, and the second term is related to winding by the vortex core in time σ. Substituting into equation (31), we find

$$\tilde{R}(k,\sigma) \simeq \frac{\sum_{n=1}^{\infty} n^{-4/3} \int_0^{\infty} |\Lambda(\rho_s)|^{-4/3} |f_n(\rho_s)|^2 \rho_s \cos(k^{2/3} \sigma n^{1/3} a^{2/3} s(\rho_s))\, \mathrm{d}\rho_s}{\sum_{n=1}^{\infty} n^{-4/3} \int_0^{\infty} |\Lambda(\rho_s)|^{-4/3} |f_n(\rho_s)|^2 \rho_s \, \mathrm{d}\rho_s}, \tag{34}$$

and so to leading order $\tilde{R}(k,\sigma)$ only depends on k and σ in the combination $k^{2/3}\sigma$, in a similar way to the inertial time scaling.

The analysis for the scalar goes through in largely the same way. Comparing the expressions for the vorticity (26) and the scalar (27), we see that the scalar and the vorticity differ by a stretching factor $S(t)$. This leads to an extra factor $(a\tau)^{-1} \simeq k^{-2/3} n^{2/3} |\Lambda(\rho_s)|^{2/3} a^{-2/3}$ in the approximation for $I_n^c(k,t)$, and we find that

$$\tilde{R}^c(k,\sigma) \simeq \frac{\sum_{n=1}^{\infty} \int_0^{\infty} |g_n(\rho_s)|^2 \rho_s \cos(k^{2/3} \sigma n^{1/3} a^{2/3} s(\rho_s))\, \mathrm{d}\rho_s}{\sum_{n=1}^{\infty} \int_0^{\infty} |g_n(\rho_s)|^2 \rho_s \, \mathrm{d}\rho_s}. \tag{35}$$

It is interesting to note that there is no dependence on the diffusivity in expression (35).

We now make a further assumption that $a \simeq (\epsilon/(15\nu))^{1/2}$, on the basis of the rms value of the strain rate in isotropic turbulence. Other values of $a^2\nu/\epsilon$ have been proposed (see [16, 20]). Letting Γ and L be the characteristic circulation and length scales respectively of the vortex core, we find that the dependence on k in expressions (34) and (35) is of the form

$$k^{2/3} \sigma \epsilon^{1/3} \left(\frac{\Gamma}{\nu} \right)^{1/3}. \tag{36}$$

Thus the winding by the vortex core and the radial motion due to stretching have led to an inertial time scale $k^{-2/3}\epsilon^{-1/3}$, although there is also a dependence on the vortex Reynolds number Γ/ν. Note that vorticity amplification due to stretching is not important to the leading order and that the preceding analysis is valid in the dissipation range as well as the inertial range.

3.4. Numerical evaluation

The integrals in expressions (22) and (23) for $\tilde{R}(k,\sigma)$ and $\tilde{R}^c(k,\sigma)$ were evaluated numerically, using an implementation of adaptive Gauss–Konrod integration in the GNU Scientific Library

[21]. It should be noted that the asymptotic solutions (26) and (27) were once again used for the non-axisymmetric vorticity and scalar fields. The results are expected to be more accurate than the asymptotic approach of section 3.3, but specific choices have to be made; for example, the precise form of $\Omega(\rho)$ must be specified.

We first define the non-dimensional quantities (indicated with an overbar), $r = \bar{r}L$, $\sigma = \bar{\sigma}/a$, $t = \bar{t}/a$, $\omega_n = \bar{\omega}_n(\bar{r}, \bar{t})\Gamma/L^2$, $c_n = \bar{c}_n(\bar{r}, \bar{t})c_c$, $\Omega = \bar{\Omega}(\bar{r})\Gamma/L^2$, $\Lambda = \bar{\Lambda}(\bar{r})\Gamma/L^3$ and $k = \bar{k}/L$. Here, L is the characteristic length scale, Γ the characteristic circulation of the vortex and c_c a characteristic value of the scalar. We also define the Kolmogorov length scale $\eta = (\nu^3/\epsilon)^{1/4}$, and estimate the strain rate as $a = (\epsilon/15\nu)^{1/2}$, where ϵ is the energy dissipation. The Schmidt number was set to unity, and the following choices were made for the two remaining non-dimensional numbers:

$$\frac{\Gamma}{\nu} = 10^7, \qquad \frac{L}{\eta} = 15^{1/4}\left(\frac{\Gamma}{\nu}\right)^{1/2}. \tag{37}$$

These values were chosen because they were found numerically to give a clear inertial range for the energy spectrum obtained from expression (13). The initial conditions for the non-axisymmetric part of the vorticity and the scalar were chosen to be

$$\begin{aligned} \bar{c}_1(\bar{r}, 0) = \bar{\omega}_1(\bar{r}, 0) &= A\exp(-\bar{r}^2), \\ \bar{c}_n(\bar{r}, 0) = \bar{\omega}_n(\bar{r}, 0) &= 0, \quad |n| > 1, \end{aligned} \tag{38}$$

where $\tilde{R}(k, \sigma)$ and $\tilde{R}^c(k, \sigma)$ are independent of the non-dimensional constant A. The azimuthally averaged angular velocity was chosen to be $\bar{\Omega}(\bar{r}) = \bar{r}^{-1/2}\exp(-\bar{r}^2)$, ensuring that $\bar{\Lambda}(\bar{r})$ is monotonic (see later in this section). The viscous diffusion of the vortex core was neglected.

The resulting graphs for $\tilde{R}(k, \sigma)$ and $\tilde{R}^c(k, \sigma)$ are shown in figures 1(a) and (b) at $\bar{k} = 200$ and figures 2(a) and (b) at $\bar{k} = 3000$, compared with their asymptotic expressions (34) and (35). Numerical evaluation of expression (13) for $E(k)$ (setting $\sigma = 0$) indicates that $\bar{k} = 200$ is representative of the inertial range and that $\bar{k} = 3000$ is representative of the dissipation range (see figure 3). The agreement between the asymptotics and the numerical results is reasonable for $\bar{k}^{2/3}\bar{\sigma}^2$ small enough, with better agreement for the higher value of $\bar{k}$. However, the main success of the asymptotic analysis is in capturing the $(\bar{k}^{2/3}\bar{\sigma})$ dependence.

Similar results were found for other choices of $\bar{\Omega}(\bar{r})$, $\bar{\omega}_n(\bar{r}, 0)$ and $\bar{c}_n(\bar{r}, 0)$, as long as $\bar{\Lambda}(\bar{r})$ was monotonic. If $\bar{\Lambda}(\bar{r})$ is not monotonic as, for example, for a Gaussian angular velocity $\bar{\Omega}(\bar{r}) = \exp(-\bar{r}^2)$, then there will be more than one point of stationary phase in the asymptotic analysis, and our results (34) and (35) are no longer valid. Numerically, we find that, for a Gaussian $\bar{\Omega}(\bar{r})$, the dependence on k and σ is of the form $(\bar{k}^{5/6}\bar{\sigma})$. Finally, it is noted that $\tilde{R}(k, \sigma)$ and $\tilde{R}^c(k, \sigma)$, calculated using the stretched-spiral vortex model, do not necessarily remain positive, unlike results from direct numerical simulations and experiments.

3.5. Vortex structures with moving centres

We are considering two-time statistics and the preceding analysis is valid only if the centres of the vortex structures remain stationary. We will now generalize to the case where the vortex structures are allowed to move with a constant velocity relative to the frame in which measurements are made. Our treatment of the sweeping effect on the vortex structures is similar to the model problem that Kraichnan [22] considered to demonstrate the effects of convection in Eulerian turbulence closure theory. Each structure in the ensemble has its own velocity, $\mathbf{U}$, with the probability distribution for this velocity assumed to be isotropic and independent of all other parameters (e.g. vortex orientation). We denote the velocity in a frame moving with the vortex structure by $\tilde{\mathbf{u}}(\mathbf{x}')$, where $\mathbf{x}'$ are structure-fixed coordinates. The velocity in the vortex

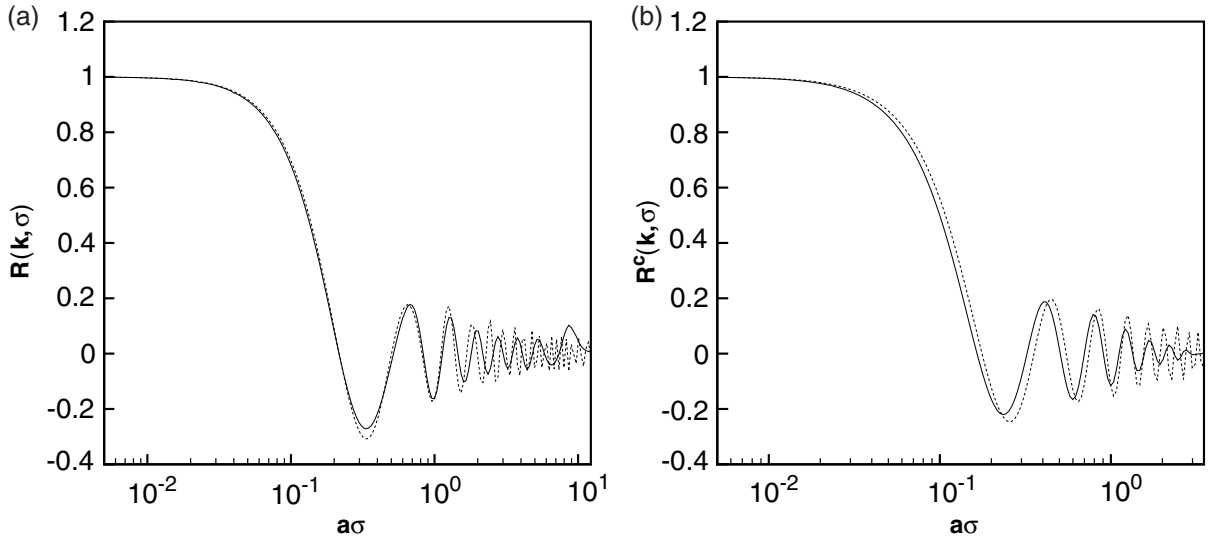

Figure 1. (a) $\tilde{R}(k,\sigma)$ and (b) $\tilde{R}^c(k,\sigma)$ for $\bar{k} = 200$ from the stretched-spiral vortex model with stationary vortex structure centres. Numerical evaluation (——) and asymptotic evaluation (- - - -).

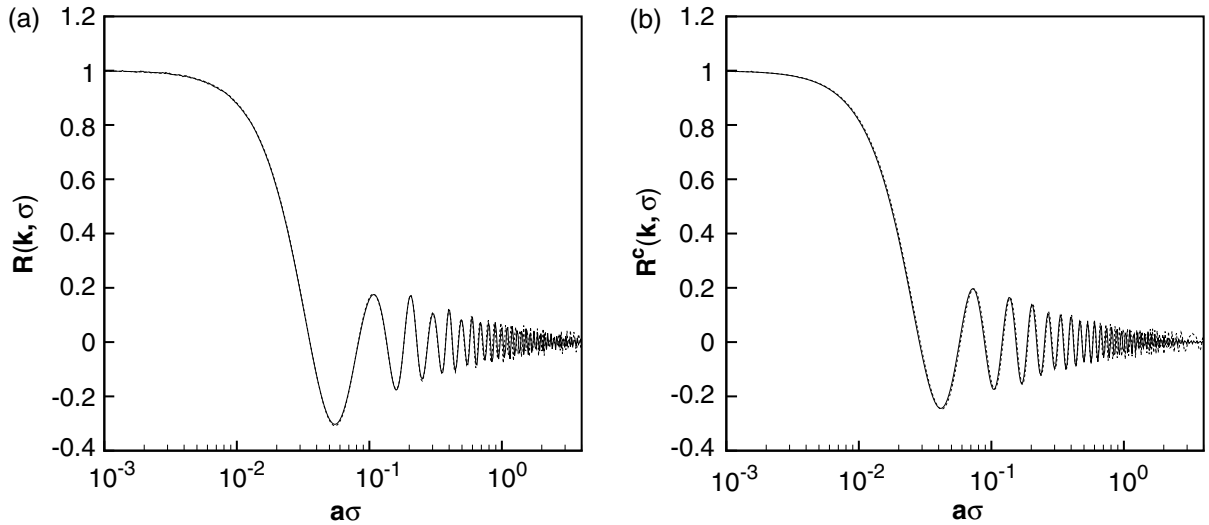

Figure 2. (a) $\tilde{R}(k,\sigma)$ and (b) $\tilde{R}^c(k,\sigma)$ for $\bar{k} = 3000$ from the stretched-spiral vortex model with stationary vortex structure centres. Numerical evaluation (——) and asymptotic evaluation (- - - -).

structure is given by $\mathbf{u}(\mathbf{x},t) = \tilde{\mathbf{u}}(\mathbf{x} - \mathbf{U}t, t) + \mathbf{U}$. The numerator in the definition of $R(k,\sigma)$, equation (5), is then given by

$$\frac{1}{(2\pi)^3}\int_S\int_V\left(\int\langle\tilde{\mathbf{u}}_i(\mathbf{x}-\mathbf{U}t,t)\tilde{\mathbf{u}}_i(\mathbf{x}-\mathbf{U}(t+\sigma)+\mathbf{r},t+\sigma)\rangle p(\mathbf{U})\,\mathrm{d}\mathbf{U}\right)\mathrm{e}^{-\mathrm{i}\mathbf{k}\cdot\mathbf{r}}\,\mathrm{d}\mathbf{r}\,\mathrm{d}\Omega_k, \tag{39}$$

where $\langle\cdot\rangle$ represents the averages over time, space and vortex orientation in the stretched-spiral vortex model. The $\int p(\mathbf{U})\,\mathrm{d}\mathbf{U}$ integral implements an average over the gross velocities of the

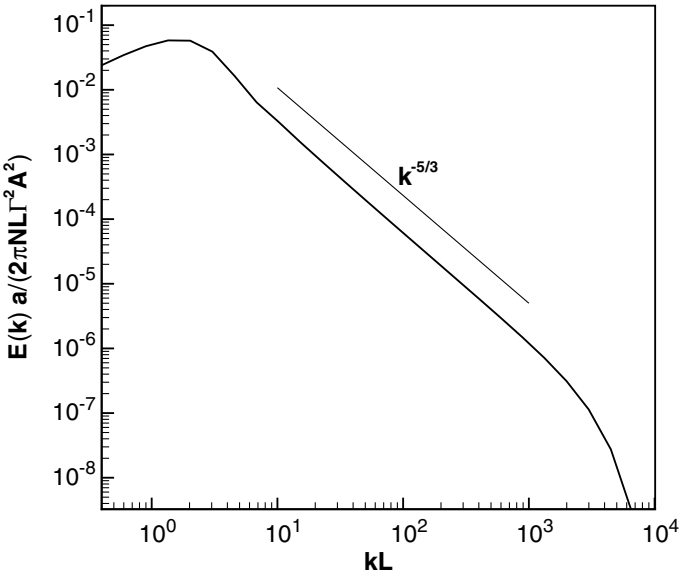

Figure 3. Energy spectrum from the non-axisymmetric vorticity for the stretched-spiral vortex model.

structures in the ensemble. The denominator in equation (5) involves single time statistics that are not influenced by $\mathbf{U}$. Making a change of the integration variables $\mathbf{r}' = \mathbf{r} - \mathbf{U}\sigma$ and $\mathbf{x}' = \mathbf{x} - \mathbf{U}t$, we find that

$$R(k,\sigma) = \left(\int p(\mathbf{U}) \mathrm{e}^{-\mathrm{i}\mathbf{k}\cdot\mathbf{U}\sigma} \, \mathrm{d}\mathbf{U} \right) \tilde{R}(k,\sigma), \tag{40}$$

where $\tilde{R}$ is the modal correlation function for vortex structures with stationary centres. We have used the fact that the $\mathbf{r}$ integration is over an infinite volume, while the $\mathbf{x}$ integral (representing a spatial average) is over an infinite interval in two directions perpendicular to the vortex axis, and the integrand is independent of the coordinate parallel to the vortex axis. The distribution of $\mathbf{U}$ is isotropic, so that we can write $p(\mathbf{U}) = P(|\mathbf{U}|/u_{gross})$ for a non-dimensional function P and a characteristic velocity u_{gross} and so $R(k,\sigma) = f(ku_{gross}\sigma)\tilde{R}(k,\sigma)$ for some function f. Thus, unsurprisingly, the constant motion of the structures has introduced a sweeping time scale $(ku_{gross})^{-1}$.

For example, if $p(\mathbf{U}) = (2\pi u_{rms}^2)^{-3/2} \exp(-|\mathbf{U}|^2/(2u_{rms}^2))$, where u_{rms} is the rms turbulent velocity, then

$$R(k,\sigma) = \exp(-k^2 u_{rms}^2 \sigma^2/2)\tilde{R}(k,\sigma). \tag{41}$$

Note that the factor $\exp(-k^2u_{rms}^2\sigma^2/2)$ is the same as Kraichnan's linearized estimate for $R(k,\sigma)$ [5]. The analysis for the scalar modal correlation function is identical and so

$$R^c(k,\sigma) = \exp(-k^2 u_{rms}^2 \sigma^2/2)\tilde{R}^c(k,\sigma), \tag{42}$$

where $\tilde{R}^c$ is the scalar modal correlation function for vortex structures with stationary centres.

Equations (41) and (42) show that the stretched-spiral vortex model provides an integrated and self-consistent treatment, in which winding and stretching in the vortex structures leads to an inertial time scale, and movement of the vortex structures leads to a sweeping time scale. Our asymptotic analysis suggests that the radial motion due to stretching is more important

than the vorticity amplification due to stretching, at least to leading order. We note that the sweeping part is the same for both the velocity and the scalar and that the factors given by (34) and (35) related to internal motion in the vortex structures are also very similar. Thus, we expect the relative importance of the inertial and sweeping time scales to be the same for the velocity and the scalar. This is in contrast to the results of Yeung and Sawford [12], who found that, in certain aspects, a hypothesis of random sweeping may be more valid for the scalar compared with the velocity.

4. Direct numerical simulation

We performed a DNS with 512^3 grid points on the QSC supercomputer to investigate the small-scale mixing of a passive scalar in a turbulent flow and to calculate the modal time correlations of the velocity and scalar fields.

4.1. Description of the DNS

The passive scalar is mixed by an incompressible, statistically homogeneous and isotropic turbulent velocity field. The passive scalar field, $c(\mathbf{x}, t)$, has a mean gradient, β, in the x_1 direction. The scalar fluctuation c' is defined by

$$c(\mathbf{x}, t) = \beta x_1 + c'(\mathbf{x}, t) \tag{43}$$

and is statistically homogeneous and axisymmetric about the x_1-axis. We solved the incompressible Navier–Stokes equations for the velocity field and the advection–diffusion equation for the scalar, using a Fourier–Galerkin pseudospectral code in a cube with periodic boundary conditions. A 3/2 dealiasing method was used for the non-linear terms in the momentum and scalar equations. A second-order explicit Runge–Kutta scheme was used for time-stepping, with integrating factors accounting for the viscous and diffusive terms. The velocity field was forced at the large scales so that it became statistically stationary in time. The method used was to force 20 Fourier modes, with wavevectors $\mathbf{k}$ such that $1 < |\mathbf{k}| < 2$ (see [23]). The forcing coefficients were chosen so that the energy injection rate $\sum \hat{\mathbf{f}}_{\mathbf{k}} \cdot \hat{\mathbf{u}}^*_{\mathbf{k}}$ is constant, where $\hat{\mathbf{f}}_{\mathbf{k}}$ and $\hat{\mathbf{u}}_{\mathbf{k}}$ are the Fourier modes of the forcing and velocity fields respectively. The mean gradient acted as the source of variance of the scalar fluctuation, so that the scalar field also became statistically stationary in time.

The modal time-correlation functions were calculated for a set of wavenumbers $\{k^i\}$ and n_{delay} time delays $\{\sigma^i\}$. The modal time-correlation functions were calculated at several times $\{T^i\}$, and an average was then taken for the final results. The intervals between the T^i values were greater than the maximum σ^i. For a given T^j, the velocity and scalar fields were needed at the n_{delay} times $t = T^j - \sigma^i$. To minimize storage requirements, the velocity and scalar fields were stored only in the wavenumber shells $\{k^i\}$ at these times. The $\{\sigma^i\}$ were chosen to be multiples of the simulation timestep. The above method requires the timestep to be fixed throughout the stationary period of the simulation and so the Courant number must be chosen to be lower than that of a simulation with a variable timestep.

Parameters describing the simulation are shown in table 1. Values are also reported for a smaller run with 256 grid points. Here, T_{eddy} is the eddy turnover time, T_{stat} the time during which the statistics are collected, R_λ the Taylor Reynolds number, Sc the Schmidt number (the ratio of the viscosity to the diffusivity), k_{max} the largest dynamically significant wavenumber, η the Kolmogorov length and R_l the Reynolds number based on the integral length scale l. The turbulent length scale is $l_\epsilon = u_{rms}^3/\epsilon$ where ϵ is the dissipation, k_0 is the smallest wavenumber and C is the Courant number.

Table 1. Simulation parameters for the stationary period of the DNS.

Grid	R_λ	T_{stat}/T_{eddy}	Sc	$k_{max}\eta$	R_l	$\langle c'^2\rangle/(\beta l_\epsilon)^2$	$k_0 l$	C
512^3	265	10.5	0.7	1.05	1901	0.45	1.00	0.48
256^3	167	9.3	0.7	1.00	779	0.38	0.99	0.51

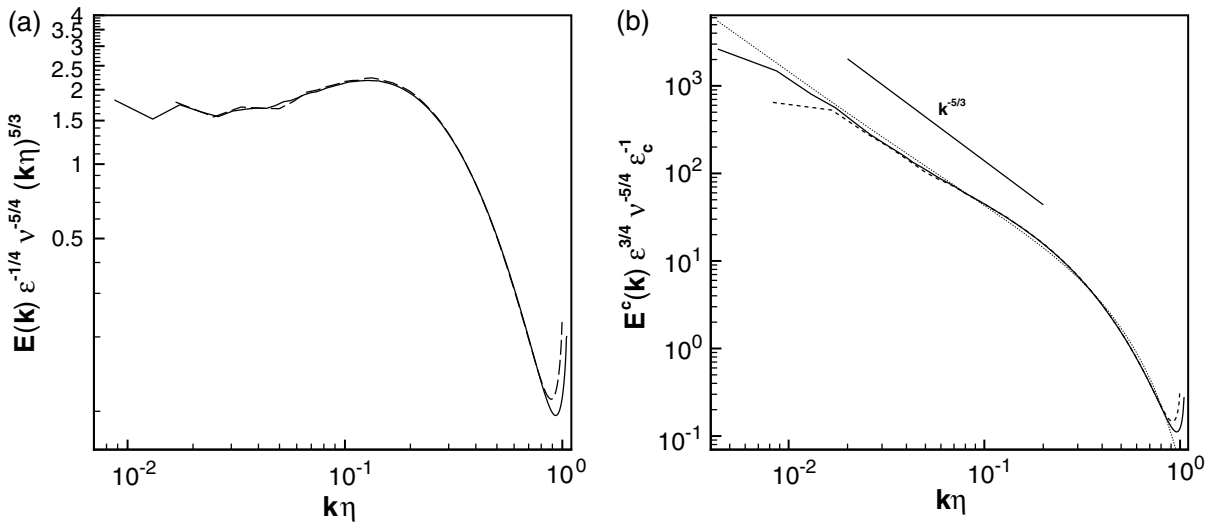

Figure 4. Spectra from the DNS at 512^3 (——) and 256^3 (- - - -): (a) energy spectra in compensated form, (b) scalar spectra compared with $k^{-5/3}$ and the stretched-spiral vortex model result from [15] (· · · · · ·).

4.2. Results of the DNS

The shell-averaged energy spectrum in compensated form is shown in figure 4(a) for both the 256^3 and 512^3 runs. The beginning of the inertial range and the bump in the dissipation range are apparent. The shell-averaged scalar spectrum $E^c(k)$ is shown in figure 4(b), where the normalization involves the scalar dissipation ϵ_c. Again, there is a bump at the beginning of the dissipation range, but the slope at the beginning of the inertial convective range is considerably shallower than $-5/3$.

Also shown in figure 4(b) is the scalar spectrum that results from the stretched-spiral vortex model calculation of Pullin and Lundgren [15]. We plot the results given by equations (107) and (108) of that paper, for a Schmidt number of 0.7. The vortex Reynolds number was chosen to be 200, noting that it should at least be below the Taylor Reynolds number of 265 in the DNS. At the current Schmidt number of 0.7, the first-order scalar dissipation, given by equation (109) of [15], could not be neglected. The result is a combination of a k^{-1} term and a $k^{-5/3}$ term, representing the first two terms in an asymptotic series. There is good agreement with the DNS result, although the DNS scalar spectrum is somewhat lower in the viscous-diffusive range. A comparison, not shown here, using a vortex Reynolds number of 1000 also gave reasonable agreement. Pullin and Lundgren [15] made a comparison with the experiment at Schmidt numbers 7 and 700, and it is interesting to see that the model seems to compare well at a Schmidt number of 0.7 as well.

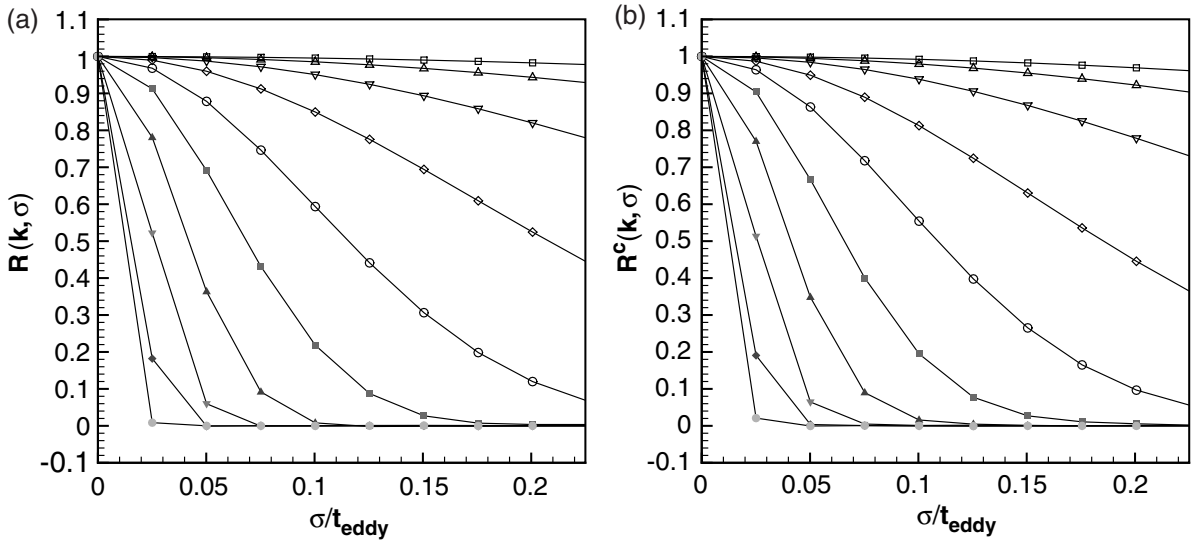

Figure 5. DNS results for the modal time-correlation function of (a) the velocity and (b) the scalar: (□) $k\eta = 0.0087$, (△) $k\eta = 0.0137$, (▽) $k\eta = 0.0216$, (◇) $k\eta = 0.0341$, (○) $k\eta = 0.0538$, (■) $k\eta = 0.0848$, (▲) $k\eta = 0.134$, (▼) $k\eta = 0.211$, (◆) $k\eta = 0.332$ and (●) $k\eta = 0.524$.

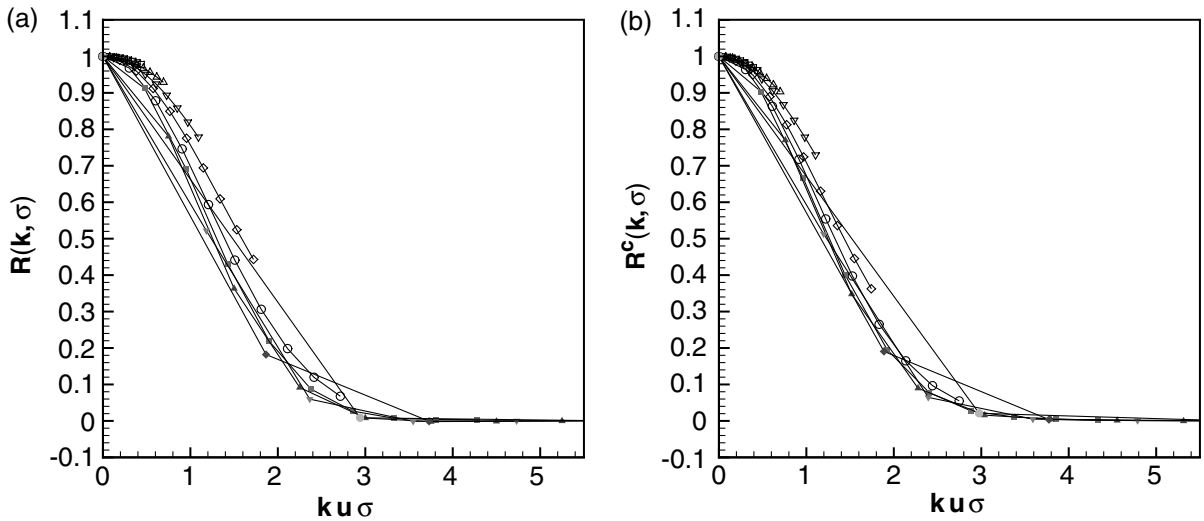

Figure 6. DNS results for the modal time-correlation function of (a) the velocity and (b) the scalar using the sweeping time scaling. See figure 5 for a key to the symbols used.

Results from the 512^3 simulation for the modal time correlation function of the velocity are shown in figure 5(a) and those for the scalar in figure 5(b). These are replotted using the sweeping time scaling in figures 6(a) and (b) and the inertial time scaling in figures 7(a) and (b). The best collapse is for the sweeping time scale for both the velocity and the scalar. The collapse occurs for wavenumbers in the inertial-convective and dissipation ranges. As was noted earlier, Yeung and Sawford [12] found that a hypothesis of random sweeping was more effective

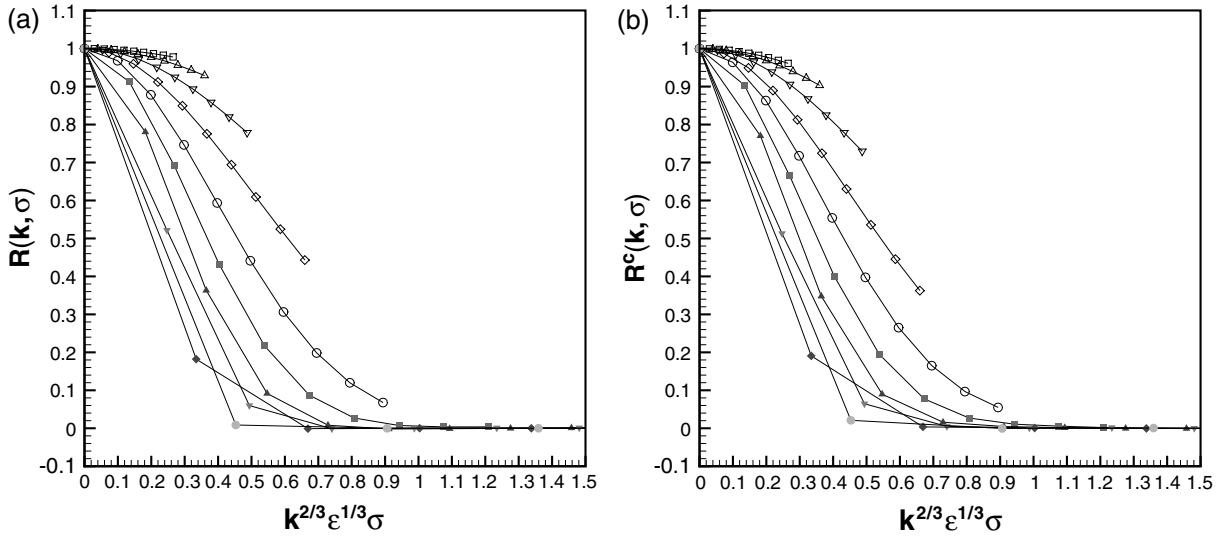

Figure 7. DNS results for the modal time-correlation function of (a) the velocity and (b) the scalar using the inertial time scaling. See figure 5 for a key to the symbols used.

for the scalar than for the velocity in some aspects. It is difficult to resolve this issue from figures 6(a) and (b) for the modal time-correlation function.

In figure 8, we compare the modal time-correlation functions for the velocity and the scalar. We see that, for a sufficiently large wavenumber, the modal time-correlation functions coincide. This is consistent with the picture of the primary decorrelation mechanism for the small-scale structures (in both the velocity and the scalar) being convection by the large-scale motions.

4.3. Comparison of the DNS and the stretched-spiral vortex model

We wish to compare the predictions of the stretched-spiral vortex model for the modal time-correlation functions with the results from the DNS. For the DNS, there was a mean scalar gradient; however, in the stretched-spiral vortex model calculation of section 3, we considered the statistically isotropic case for the sake of simplicity. This discrepancy is not expected to be significant because of the shell averages involved in the definition of the modal time-correlation functions.

It is necessary to choose some parameters to characterize the vortex structures in the model. We used u_{rms}, ϵ and ν from the DNS with $a = (\epsilon/15\nu)^{1/2}$, and let the characteristic length scale of the vortex structures, L, be the Taylor length scale. We again set the vortex Reynolds number Γ/ν to 200. The initial vorticity and scalar profiles were the same as used in section 3.4. The results for the stretched-spiral vortex model were calculated using numerical evaluation of (22) and (23) for $\tilde{R}(k,\sigma)$ and $\tilde{R}^c(k,\sigma)$ in expressions (41) and (42).

The comparison is made with the results of the DNS at 512^3 gridpoints. The effect of the change in Reynolds number between the two DNS runs was unclear because the wavenumber and delay times were at different normalized values and so the results of the DNS at 256^3 for the modal time-correlation functions are not presented here.

In figures 9 and 10, the DNS and stretched-spiral vortex model results are compared for representative wavenumbers $k\eta = 0.0848$ and 0.211. These wavenumbers correspond to $kL = 2.72$ and 6.76, respectively. We do not consider smaller values of kL since the stretched-spiral

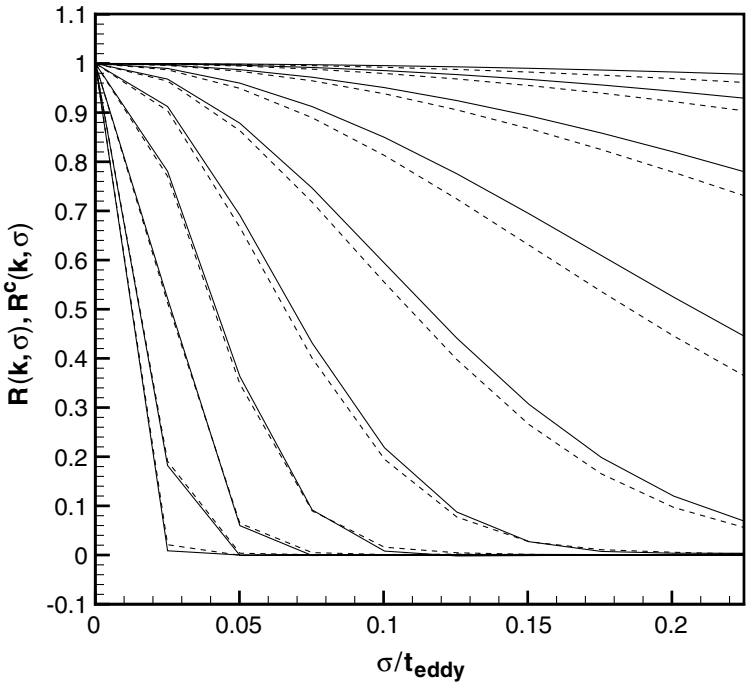

Figure 8. Comparison of DNS results for the modal time-correlation function of the velocity (——) and the scalar (- - - -) using the same wavenumbers as in figure 5.

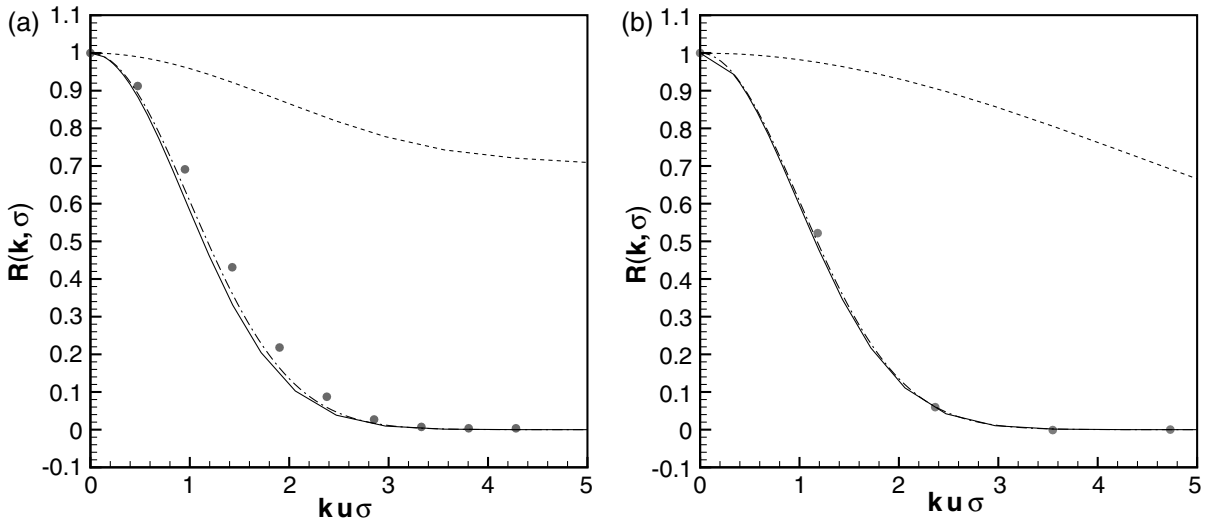

Figure 9. $R(k,\sigma)$ at (a) $k\eta = 0.0848$ and (b) $k\eta = 0.211$: DNS results (●) and stretched-spiral vortex model (——). Also shown are $\exp(-k^2u_{rms}^2\sigma^2/2)$ (— · —) and $\tilde{R}(k,\sigma)$ (- - - -).

vortex model is only considered appropriate for the fine scales within the vortex structures. Also shown are the convective part $\exp(-k^2u_{rms}^2\sigma^2/2)$ and the factors $\tilde{R}(k,\sigma)$ and $\tilde{R}^c(k,\sigma)$ related to internal motion within the vortex structures, which make up the stretched-spiral vortex model results. Clearly, for these wavenumbers, the convective part is dominant and so the stretched-spiral vortex model results collapse well with the sweeping time scale, but not perfectly. It is

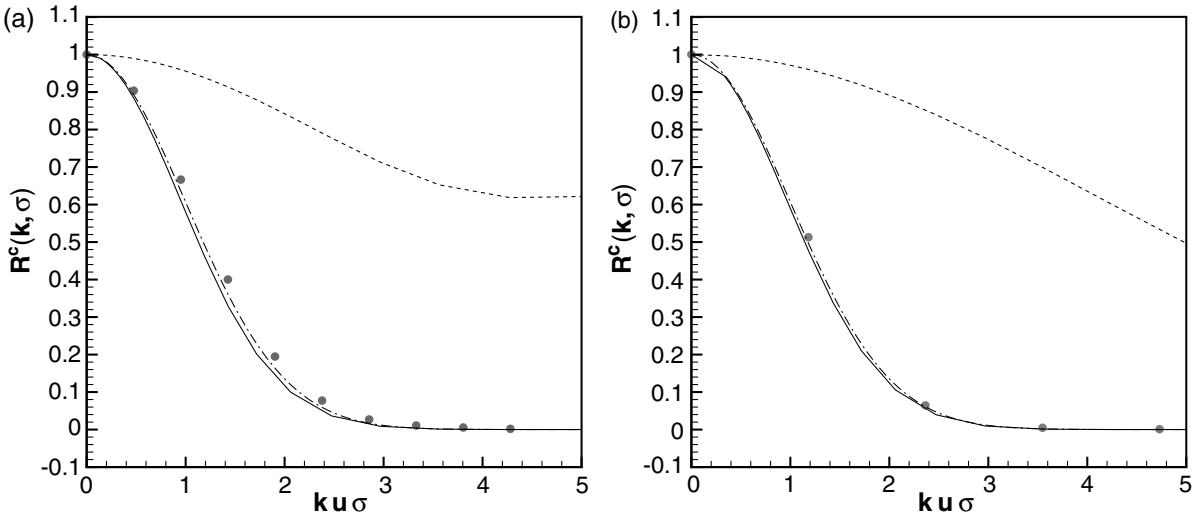

Figure 10. $R^c(k,\sigma)$ at (a) $k\eta = 0.0848$ and (b) $k\eta = 0.211$: DNS results (●) and stretched-spiral vortex model (——). Also shown are $\exp(-k^2u_{rms}^2\sigma^2/2)$ (— · —) and $\tilde{R}^c_{stat}(k,\sigma)$ (- - - -).

important to note that, for other Reynolds numbers and other values of the parameters (e.g. the vortex length scale L), the factors related to internal motion within the vortex structures may be more significant.

5. Concluding remarks

The stretched-spiral vortex model has been shown to predict two characteristic time scales for the velocity and scalar modal time-correlation functions. An inertial time scale arises from the winding by the vortex cores and the radial motion caused by axial stretching of the vortex structures. A sweeping time scale arises from the movement of the centres of the vortex structures. Thus the model provides an integrated treatment, resulting in both of these characteristic time scales.

Many studies have been performed on the modal time-correlation function of the velocity field; however, here we have also considered the modal time-correlation function of a passive scalar. The stretched-spiral vortex model predicts a similar form for both functions, and this is borne out by results from the DNS.

The asymptotic evaluation of the stretched-spiral vortex model result for the modal time correlation function of the scalar was found to be independent of the scalar diffusivity. The dependence of the scalar modal time-correlation function on the scalar diffusivity could be investigated further using DNS at a range of Schmidt numbers.

Acknowledgments

PAOG and DIP were supported in part by the National Science Foundation under grant CTS-0227881. The DNS was performed on the QSC supercomputer and was supported by the Academic Strategic Alliances Program of the Accelerated Strategic Computing Initiative (ASCI/ASAP) under subcontract no. B341492 of DOE contract W-7405-ENG-48.

Appendix A. Behaviour of the modal time-correlation function at zero delay time

Here, we will show how the choice of normalization used in definition (3) of the modal time-correlation function compensates for the effect of non-stationarity of the turbulent velocity field, at least for a sufficiently small delay time σ. Consider the derivative of $\mathcal{R}_{jj}(\mathbf{r},t,\sigma)$ with respect to σ evaluated at $\sigma=0$,

$$\frac{\partial}{\partial\sigma}\mathcal{R}_{jj}(\mathbf{r},t,\sigma)\bigg|_{\sigma=0} = \overline{u_j(\mathbf{x},t)\frac{\partial}{\partial\sigma}u_j(\mathbf{x}+\mathbf{r},t+\sigma)\bigg|_{\sigma=0}} = \overline{u_j(\mathbf{x},t)\frac{\partial}{\partial t}u_j(\mathbf{x}+\mathbf{r},t)}. \tag{A.1}$$

The assumption of homogeneity then gives

$$\frac{\partial}{\partial\sigma}\mathcal{R}_{jj}(-\mathbf{r},t,\sigma)\bigg|_{\sigma=0} = \overline{u_j(\mathbf{x},t)\frac{\partial}{\partial t}u_j(\mathbf{x}-\mathbf{r},t)} = \overline{u_j(\mathbf{x}+\mathbf{r},t)\frac{\partial}{\partial t}u_j(\mathbf{x},t)}, \tag{A.2}$$

so that

$$\frac{\partial}{\partial\sigma}\mathcal{R}_{jj}(\mathbf{r},t,\sigma)\bigg|_{\sigma=0} + \frac{\partial}{\partial\sigma}\mathcal{R}_{jj}(-\mathbf{r},t,\sigma)\bigg|_{\sigma=0} = \frac{\partial}{\partial t}\mathcal{R}_{jj}(\mathbf{r},t,0). \tag{A.3}$$

Then, we have that

$$\begin{aligned}\frac{\partial}{\partial\sigma}Q_{jj}(k,t,\sigma)\bigg|_{\sigma=0} &= \frac{1}{(2\pi)^3}\int_S\int_V\left(-\frac{\partial}{\partial\sigma}\mathcal{R}_{jj}(-\mathbf{r},t,\sigma)\bigg|_{\sigma=0}+\frac{\partial}{\partial t}\mathcal{R}_{jj}(\mathbf{r},t,0)\right)\mathrm{e}^{-\mathrm{i}\mathbf{k}\cdot\mathbf{r}}\,\mathrm{d}\mathbf{r}\,\mathrm{d}\Omega_k\\ &= \frac{1}{(2\pi)^3}\int_S\int_V\frac{\partial}{\partial\sigma}\mathcal{R}_{jj}(\mathbf{r},t,\sigma)\bigg|_{\sigma=0}\mathrm{e}^{-\mathrm{i}\mathbf{k}\cdot\mathbf{r}}\,\mathrm{d}\mathbf{r}\,\mathrm{d}\Omega_k + 2\frac{\partial}{\partial t}E(k,t)\\ &= -\frac{\partial}{\partial\sigma}Q_{jj}(k,t,\sigma)\bigg|_{\sigma=0} + 2\frac{\partial}{\partial t}E(k,t),\end{aligned} \tag{A.4}$$

where we have made a change of integration variables from $\mathbf{r}$ to $-\mathbf{r}$ and from $\mathbf{k}$ to $-\mathbf{k}$. Thus, we have the result,

$$\frac{\partial}{\partial\sigma}R(k,t,\sigma)\bigg|_{\sigma=0} = \frac{(\partial/\partial\sigma)Q_{jj}(k,t,\sigma)|_{\sigma=0}}{2E(k,t)} - \frac{Q_{jj}(k,t,0)}{4E(k,t)^2}\frac{\partial}{\partial t}E(k,t) = 0. \tag{A.5}$$

Appendix B. Asymptotic evaluation of $h_n(\rho_s') - h_n(\rho_s)$

We wish to find $h_n(\rho_s') - h_n(\rho_s)$ to leading order in the small parameters $\epsilon_1 = a\sigma$ and $\epsilon_2 = 1/(a\tau)$. The assumption of small ϵ_1 means that we are considering delay times smaller than the stretching time of the vortex structures. This will not be restrictive if $\tilde{R}(k,\sigma)$ decays on time scales faster than $1/a$, a condition that may be checked *a posteriori*. The assumption of small ϵ_2 is not restrictive as $(a\tau)$ must be large for solutions (26) and (27) to be valid. Using equation (30) to relate τ' to τ, we find that

$$a\tau' = a\tau + (a\sigma)(a\tau) + \mathrm{O}(\epsilon_1) + \mathrm{O}(\epsilon_1^2/\epsilon_2). \tag{B.1}$$

To relate ρ_s' to ρ_s, we start with the exact relation $\Lambda(\rho_s')a\tau'(1+a\tau')^{1/2} = \Lambda(\rho_s)a\tau(1+a\tau)^{1/2}$. Substituting for $(a\tau')$ from equation (B.1), we find

$$\Lambda(\rho_s') = \Lambda(\rho_s)(1-\tfrac{3}{2}a\sigma) + \mathrm{O}(\epsilon_1^2) + \mathrm{O}(\epsilon_1\epsilon_2). \tag{B.2}$$

Taylor expanding $\Lambda(\rho_s')$ about ρ_s and comparing with equation (B.2), we find

$$\rho_s' = \rho_s - \frac{3}{2}(a\sigma)\frac{\Lambda(\rho_s)}{\Delta(\rho_s)} + \mathrm{O}(\epsilon_1^2) + \mathrm{O}(\epsilon_1\epsilon_2). \tag{B.3}$$

Finally, Taylor expanding $\Omega(\rho_s')$ about ρ_s and using equation (B.3) gives

$$\Omega(\rho_s') = \Omega(\rho_s) - \frac{3}{2}(a\sigma)\frac{\Lambda(\rho_s)^2}{\Delta(\rho_s)} + \mathrm{O}(\epsilon_1^2) + \mathrm{O}(\epsilon_1\epsilon_2). \tag{B.4}$$

Substituting for τ', ρ_s' and $\Omega(\rho_s')$ in the definition of $h_n(\rho_s')$ gives

$$h_n(\rho_s') - h_n(\rho_s) = a\sigma\left(-n\Omega(\rho_s)\tau + \frac{3n\tau\Lambda(\rho_s)^2}{2\Delta(\rho_s)} + \frac{k}{(a\tau)^{1/2}}\left(\frac{3\Lambda(\rho_s)}{2\Delta(\rho_s)} + \frac{\rho_s}{2}\right)\right) + \mathrm{O}(\epsilon_1) + \mathrm{O}(\epsilon_1^2/\epsilon_2), \tag{B.5}$$

where we have used that (kL) is $\mathrm{O}(\epsilon_2^{-3/2})$ from equation (29). Then, substituting for τ using equation (29) and after some algebra, we find

$$h_n(\rho_s') - h_n(\rho_s) = k^{2/3}\sigma n^{1/3}a^{2/3}s(\rho_s) + \mathrm{O}((kL)^{2/3}(a\sigma)^2) + \mathrm{O}(a\sigma), \tag{B.6}$$

where

$$s(\rho_s) = \left(\frac{|\Lambda(\rho_s)|^{1/3}\rho_s}{2} - \frac{\Omega(\rho)}{|\Lambda(\rho_s)|^{2/3}}\right), \tag{B.7}$$

and we have assumed $\Lambda(\rho) = -|\Lambda(\rho)|$. There has been an important cancellation of the two terms from equation (B.5) that relates to movement of the points of stationary phase in time σ. We can interpret the remaining two terms as follows. The first term on the right-hand side of (B.7) is caused by the radial motion that occurs in time σ due to stretching, and the second term is attributable to the winding that occurs in time σ.

References

[1] Sanada T and Shanmugasundaram V 1992 Random sweeping effect in isotropic numerical turbulence *Phys. Fluids* A **4** 1245–50

[2] Orszag S A and Patterson G S 1992 Numerical simulation of three-dimensional homogeneous isotropic turbulence *Phys. Rev. Lett.* **28** 76–9

[3] Gotoh T, Rogallo R S, Herring J R and Kraichnan R H 1993 Lagrangian velocity correlations in homogeneous isotropic turbulence *Phys. Fluids* A **5** 2846–64

[4] Kaneda Y, Ishihara T and Gotoh K 1999 Taylor expansions in powers of time of Lagrangian and Eulerian two-point two-time velocity correlations in turbulence *Phys. Fluids* **11** 2154–66

[5] Kraichnan R H 1959 The structure of isotropic turbulence at very high Reynolds numbers *J. Fluid Mech.* **5** 497–543

[6] Gleeson J P 2000 A closure method for random advection of a passive scalar *Phys. Fluids* **12** 1472–84

[7] Zhou Y and Rubinstein R 1996 Sweeping and straining effects in sound generation by high Reynolds number isotropic turbulence *Phys. Fluids* **8** 647–9

[8] Comte-Bellot G and Corrsin S 1971 Simple Eulerian time correlation of full- and narrow-band velocity signals in grid-generated, 'isotropic' turbulence *J. Fluid Mech.* **48** 273–337

[9] McComb W D, Shanmugasundaram V and Hutchinson P 1989 Velocity-derivative skewness and two-time velocity correlations of isotropic turbulence as predicted by the LET theory *J. Fluid Mech.* **208** 91–114

[10] Tennekes H 1975 Eulerian and Lagrangian time microscales in isotropic turbulence *J. Fluid Mech.* **67** 561–7

[11] Malik N A and Vassilicos J C 1996 Eulerian and Lagrangian scaling properties of randomly advected vortex tubes *J. Fluid Mech.* **326** 417–36

[12] Yeung P K and Sawford B L 2002 Random-sweeping hypothesis for passive scalars in isotropic turbulence *J. Fluid Mech.* **459** 129–38
[13] Lundgren T S 1982 Strained spiral vortex model for turbulent fine structure *Phys. Fluids* **25** 2193–203
[14] Jimenez J, Wray A A, Saffman P G and Rogallo R S 1993 The structure of intense vorticity in isotropic turbulence *J. Fluid Mech.* **255** 65–90
[15] Pullin D I and Lundgren T S 2001 Axial motion and scalar transport in stretched spiral vortices *Phys. Fluids* **13** 2553–63
[16] Pullin D I and Saffman P G 1993 On the Lundgren–Townsend model of turbulent fine scales *Phys. Fluids* A **5** 126–45
[17] Pullin D I and Saffman P G 1994 Reynolds stresses and one-dimensional spectra for a vortex model of homogeneous anisotropic turbulence *Phys. Fluids* **6** 1787–96
[18] O'Gorman P A and Pullin D I 2003 The velocity-scalar cross spectrum of stretched spiral vortices *Phys. Fluids* **15** 280–91
[19] Gomez T, Politano H, Pouquet A and Larcheveque M 2001 Spiral vortices in compressible turbulent flows *Phys. Fluids* **13** 2065–75
[20] Townsend A A 1951 On the fine-scale structure of turbulence *Proc. R. Soc.* A **208** 534–42
[21] Galassi M *et al* 2001 *GNU Scientific Library Reference Manual* 2nd edn. Network Theory Ltd
[22] Kraichnan R H 1964 Kolmogorov's hypotheses and Eulerian turbulence theory *Phys. Fluids* **7** 1723–34
[23] Misra A and Pullin D I 1997 A vortex-based subgrid stress model for large-eddy simulation *Phys. Fluids* **9** 2443–54